Journal of Engineering Technology

Volume 7, Special Issue (Internet of Things),Oct. 2018, PP. 145-158

RESEARCH ARTICLE -ENGINEERNG TECHNOLOGY ASEE

Robustness in Adaptive Pattern Recognition

Zhi-Ren Tsai[*a], Han-Wei Zhang[b], Chin-Teng Lin[c,d,e]

[a] Department of Computer Science & Information Engineering, Asia University, Taichung, Taiwan. Department of Medical Research, China Medical University Hospital, China Medical University, Taichung, Taiwan.
[b] Institute of Electrical Control Engineering, Department of Electrical and Computer Engineering, National Chiao Tung University, Hsinchu, Taiwan.
[c]Brain Research Center, National Chiao Tung University, Hsinchu, Taiwan.
[d]Institute of Electrical Control Engineering, Department of Electrical and Computer Engineering, National Chiao Tung University, Hsinchu, Taiwan.
[e] Centre for Artificial Intelligence School of Software, Faculty of Engineering & IT, University of Technology Sydney Broadway 2007, New South Wales, Australia.

*Corresponding author

Abstract: This study aims to propose color model-based control of a nonlinear system with significant light disturbance effects for an image processing problem and a design methodology based on Lyapunov analysis. The proposed scheme comprises an adaptive neuron control component with error effects and a supervisory control component to enhance robustness against light emitting diode disturbances and image model uncertainties. In addition, an effective supervised adaptive control theory is employed to address the image identification problem. Experimental results obtained from a practical marker identification system using a Microsoft Kinect image sensor demonstrate that the proposed image identification technique has excellent performance in comparison with two traditional image processing methods as static and dynamic CIELab color identification. In addition, the feedforward term of the photoresistor further improves image identification performance. Hence, the primary contribution of this study is a more adaptive and robust method that is applicable to the color-based image processing problem.

Keywords: Adaptive CieLab criterion, robust customized-marker identification, dimmable LED.

Journal of Engineering Technology

Volume 7, Special Issue (Internet of Things),Oct. 2018, PP. 145-158

RESEARCH ARTICLE -ENGINEERNG TECHNOLOGY ASEE

1 Introduction

1.1 Image processing robustness problem

Artificial intelligence (AI) and adaptive systems [1-4] have attracted considerable attention from academic and industrial computer vision and digital image processing communities owing to their absolute robustness against uncertainty [5-7], and many successful applications of such systems have been realized. However, AI-type adaptive control techniques have not been applied to solve the robustness problem in image processing [8-10]. Thus, most recognition systems such as machine vision systems focus on processing images without light disturbance. However, the identification result from an input image under ambient light conditions [11] and in complex environments [12] may contain various dynamic light disturbances. The situation becomes more difficult when a color marker is disturbed by lights, shadows, and background colors.

In image processing, lack of stability due to light disturbance in a complex environment is a significant issue, e.g., light disturbance affects pattern recognition. In this study, we propose a system in which light disturbance functions as a feedforward controller to improve the recognition result of a computer vision system. The proposed marker plant, as shown in Figure 1, uses a photoresistor, phototransistor, or photodiode to measure the average light disturbance intensity; it is a marker-based plant for an application that guides a robot. In the proposed method, light emitting diode (LED) brightness is only used to test the robustness of marker-based system or demonstrate the effect of light disturbance. Thus, LEDs are not required for this method.

The use of closed-loop and feedforward-loop stabilization in marker systems has received considerable attention. Specifically, brightness-based feedforward input has been used to achieve robust guidance in visual-servo robot applications because, in such applications, the varying light intensity is a major source of instability. In addition, various image segmentation techniques and applications have been proposed [13-15]. However, till date, previous pattern recognition and segmentation studies have not addressed stability issues.

1.2 Neuron stability problem

The system identification [4] proposed in the recent years is typically based on heuristic stochastic algorithms that solve optimization problems [16-19]. However, such heuristic stochastic schemes require significant computation time. Thus, in this study, a rapid mechanism with global optimal abilities is proposed in Eq. (7). Till date, the color model-based adaptive control and multi-input multi-output (MIMO) neuron stability problems for robust image processing applications remain unsolved, which may be a bottleneck for the application of image processing in robotics. Thus, the primary contributions of this study are the related techniques shown in Figure 1.

Journal of Engineering Technology

Volume 7, Special Issue (Internet of Things),Oct. 2018, PP. 145-158

RESEARCH ARTICLE -ENGINEERNG TECHNOLOGY ASEE

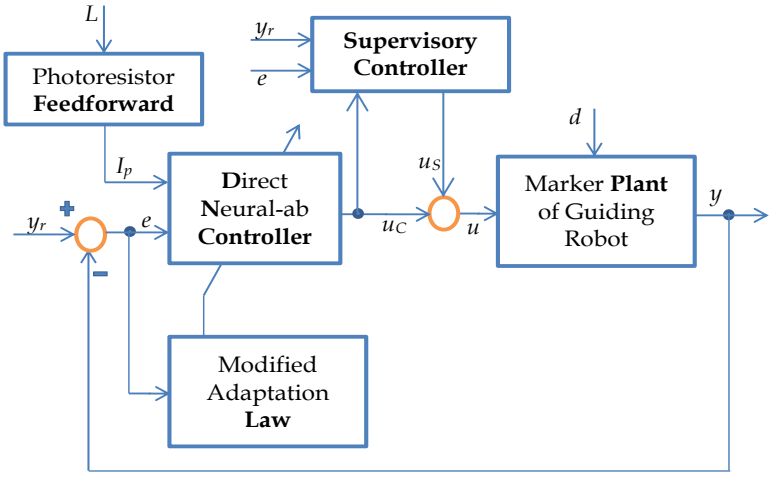

Figure 1. Image processing system structure

1.3 Customized color marker identification

In this study, a particular class of customized nonlinear color marker identification systems was considered based on a neuron-based controller, which we refer to as the Direct Neuron-ab Controller (DNC), where {a,b} are from the CIELab [15, 20, 21] color model without intensity {L}. The new color model-based adaptation law has auto-tuning neurons, where both error effect and feedforward terms are included explicitly. Robustness and stability conditions are derived from Lyapunov functions to design the proposed supervised adaptation scheme using the DNC. Although hands, fingers, faces, and human bodies [22] have been used as markers, they do not belong to the kind of customized marker as QR code. This customized marker, which includes colors and codes, has the following advantages: (1) it can be fixed to a given position for positioning applications; (2) its size can be changed, e.g., to guide a distant robot; and (3) its features can be designed to enable robust identification using colors or codes.

1.4 Color spaces

In this study, two basic colors are assumed for the proposed marker identification method. The CIELab color space [15] is the best choice for the proposed method. By exploiting a dynamic control concept, the proposed method improves the static identification parameters of the CIELab color space. Hence, this study faces an image identification problem that is solved through control compensation and that presents experimental results with various LED lights. In other words, we attempted to determine if the proposed approach can demonstrate correct estimations by illustrating the convergence trajectories of the identification parameters and the marker results under wide-ranging LED intensity conditions to realize varied environment lights.

To show a detailed training and testing methodology of the classifier from the data samples, the following algorithm includes feature extraction:

Step 1: Acquire image samples using a camera and control varied LED intensities.

Step 2: Calculate the sample colors in the CIELab color space and in the varied light intensities that are collected in the sample images for the color regions of targets (objects) that constitute a marker in each frame.

Step 3: For training purposes, the color model without the intensity part (array) means only {**a}** and {**b}** parts (arrays) of the CIELab color space are used to improve the robustness of classifier. The limited ranges of average value (feature 1) a* of {**a**} and the average value (feature 2) b* of {**b**} are decided by the two extreme situations of the darkest and brightest cases for the same classifier. Hence, the initial two features of each target should be in the specific ranges.

Step 4: For testing purposes, we classify each pixel using the nearest neighbor rule and an adaptation law is proposed in the following design. Each color target of a marker now has an a* and a b* which need to be adapted by this adaptation law. We can classify each pixel in the camera's image by calculating the Euclidean distance between that pixel and each color target of the marker. The smallest distance signifies that the pixel most closely matches that color target of the marker. For example, if the distance between a pixel and the red color target of the marker is the smallest, then the pixel would be labeled as a red pixel.

2 Problem Formulation

As discussed in the literature [15], this pattern (signal in pixel type) recognition problem is difficult in two ways. First, due to the variation in light (Figure 2) and background (noise in pixel type), the images are discolored, disturbed, and contain noise. Second, images captured from different views and poses, as well as the others in [15], easily change the shapes and sizes of the markers in the images due to skewing of the omnidirectional robot with a Kinect sensor [15] that moves on a rocky or uneven road.

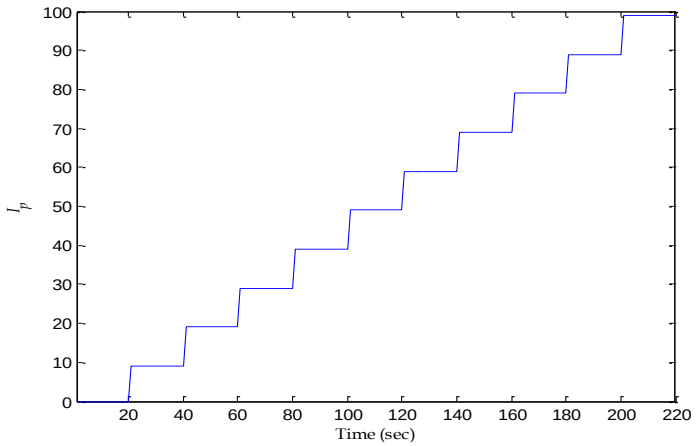

Figure 2. Feedforward input for the following Cases 1–3 in Section 4.

The above issues leave the correspondence search in different views prone to mistakes. Thus, the following design is proposed. The generalized nonlinear MIMO control system dynamics for an image identification problem are expressed as:

Journal of Engineering Technology

Volume 7, Special Issue (Internet of Things),Oct. 2018, PP. 145-158

RESEARCH ARTICLE -ENGINEERNG TECHNOLOGY ASEE

$$x_i^{(n_i)}(t) = f_i(X_i) + c_i \cdot u_i(t, I_p(L,t,\tau)) + c_i d_i(t),\ y_i = x_i, \text{ for } i = 1,2,...,m, \quad (1)$$

where L is the LED light, I_p is measurable input at time varying t, τ is measurement delay, $d = [d_1(t), d_2(t),..., d_m(t)]^T$ is a noise vector, where $d_1 \in \Re^{q_1 \times 1}$, $d_2 \in \Re^{q_2 \times 1}$,…, and $d_m \in \Re^{q_m \times 1}$, and $c_1 \in \Re^{1 \times q_1}$, $c_2 \in \Re^{1 \times q_2}$, …, and $c_m \in \Re^{1 \times q_m}$ are scaling vectors of sub-controllers $u_1 \in \Re^{q_1 \times 1}$, $u_2 \in \Re^{q_2 \times 1}$,…, and $u_m \in \Re^{q_m \times 1}$, respectively. Note that the unknown positive constants $c_1, c_2,..., c_m$ are assumed, and the values are $q_1 = q_2 = ... = q_m = 2$ if the marker includes two objects. In other words, $u_1 = [\mathrm{a}_1(I_p, e_1(t)), \mathrm{b}_1(I_p, e_1(t))]^T$, $u_2 = [\mathrm{a}_2(I_p, e_2(t)), \mathrm{b}_2(I_p, e_2(t))]^T$, …, and $u_m = [\mathrm{a}_m(I_p, e_m(t)), \mathrm{b}_m(I_p, e_m(t))]^T$. However, the proposed control method can support the other setting values. The complete controller is expressed as follows.

$$u(t) = [u_1^T, u_2^T,..., u_m^T]^T$$

is a type of special control input related to the $\{\mathrm{a}_1, \mathrm{b}_1, \mathrm{a}_2, \mathrm{b}_2,...\}$ color model without intensity and a defined tracking error vector $e(t) = y_r - y$ of round property (RP) [15]. To avoid unclear variables definitions, such as *RP_blue* and *RP_orange* $\in \mathrm{Rounding\ Property(RP)}$ for a given marker, we followed the methods described in the literature [15]. However, its robustness and adaptation functions are added to the system [15] with LED disturbance.

Note that y_r is a desired output vector, d is an unknown but bounded and varied environment light disturbance vector with $|d_1(t)| \le d_{1U}$, $|d_2(t)| \le d_{2U}$, …, and $|d_m(t)| \le d_{mU}$. $I_p(L,t,\tau)$ is a predictable disturbance with time-varying delay τ by a photoresistor, where L is the LED brightness with d. $x^{(n)}(t) = [x_1^{(n_1)}, x_2^{(n_2)},..., x_m^{(n_m)}]^T$ is a high-order differential vector, and $f(X) = [f_1(X_1), f_2(X_2),..., f_m(X_m)]^T$ is a nonlinear function vector of the system. $x(t) = y = [y_1, y_2,..., y_m]^T$ is an output vector of the system that represents a defined RP vector of a marker [15]. Furthermore, $X = [X_1, X_2,..., X_m]^T$ is designed as the state vector of the nonlinear system, where

$$X_i = [x_i(t), \dot{x}_i(t),..., x_i^{(n_i-1)}(t)] = [x_{i1}(t), x_{i2}(t),..., x_{in_i}(t)], \text{ for } i = 1,2,...,m.$$

3. Specific Controller Design

First, a desired output vector of RP for blue, orange, and other color objects that comprise a marker is defined as $y_r = [y_{r1}, y_{r2},..., y_{rm}]^T$, and the error vector is defined as $e = y_r - x$. Then, the recognition performance index (RPI) is defined as the summation of the absolute error $|e|$.

Next, the definitions of

Journal of Engineering Technology

Volume 7, Special Issue (Internet of Things),Oct. 2018, PP. 145-158

RESEARCH ARTICLE -ENGINEERNG TECHNOLOGY ASEE

$Y_r = [y_{r1}, \dot{y}_{r1}, ..., y_{r1}^{(n_1-1)}, y_{r2}, \dot{y}_{r2}, ..., y_{r2}^{(n_2-1)}, ..., y_{rm}, \dot{y}_{rm}, ..., y_{rm}^{(n_m-1)}]^T$ and $E = [E_1, E_2, ..., E_m]^T$ are given, where $E_1 = [e_1, \dot{e}_1, ..., e_1^{(n_1-1)}]$, $E_2 = [e_2, \dot{e}_2, ..., e_2^{(n_2-1)}]$, …, and $E_m = [e_m, \dot{e}_m, ..., e_m^{(n_m-1)}]$.

Assume the selection of a gain vector $K = [K_1, K_2, ..., K_m]^T$, where $K_1 = [k_{10}, k_{11}, ..., k_{1(n_1-1)}]$, $K_2 = [k_{20}, k_{21}, ..., k_{2(n_2-1)}]$, …, and $K_m = [k_{m0}, k_{m1}, ..., k_{m(n_m-1)}]$, such that all roots of

$s^{n_1} + k_{1(n_1-1)}s^{n_1-1} + ... + k_{11}s + k_{10} = 0$, $s^{n_2} + k_{2(n_2-1)}s^{n_2-1} + ... + k_{21}s + k_{20} = 0$, …, and

$s^{n_m} + k_{m(n_m-1)}s^{n_m-1} + ... + k_{m1}s + k_{m0} = 0$ are in the open left-half complex plane.

Then, the proposed control law $u(t)$ is given and specified for an example image processing system (Figure 1) by

$$u(t) = u_C(E, \theta) + u_S, \tag{2}$$

where $u_C = [u_{C1}, u_{C2}, ..., u_{Cm}]^T$ is an adaptive control law designed by a parallel distributed rule and $u_S = [u_{S1}, u_{S2}, ..., u_{Sm}]^T$ is a supervisory control law that enhances the robustness of the closed-loop system and improves transient performance by maintaining system states in some pre-specified region. The adaptive control law and parallel distributed rule are defined as

$$u_i^{*T} = c_i^+[-f_i + y_{ri}^{(n_i)} + K_i^T E_i], \text{ for } i = 1,2,...,m, \tag{3}$$

$$u_{Ci}^T(\theta_i) = [\mathbf{a}_i, \mathbf{b}_i]^T, \text{ for } i = 1,2,...,m, \tag{4}$$

where $c_1^+, c_2^+, ..., c_m^+ \in \Re^{2\times 1}$ if the marker comprises two objects. Here $u^* = [u_1^*, u_2^*, ..., u_m^*]^T$ is an ideal and global optimal controller and is replaced as $u_C(t)$ by a specific and designable neural control model as follows.

$$\mathbf{a}_i = \frac{\alpha_{ai} \cdot [1 - \exp(\overline{\beta}_{ai} \cdot (I_p + \eta_{ai} e_i + \overline{\phi}_{ai}))]}{1 + \exp(\overline{\beta}_{ai} \cdot (I_p + \eta_{ai} e_i + \overline{\phi}_{ai}))} + \varphi_{ai},$$

$$\mathbf{b}_i = \frac{\alpha_{bi} \cdot [1 - \exp(\overline{\beta}_{bi} \cdot (I_p + \eta_{bi} e_i + \overline{\phi}_{bi}))]}{1 + \exp(\overline{\beta}_{bi} \cdot (I_p + \eta_{bi} e_i + \overline{\phi}_{bi}))} + \varphi_{bi}, \tag{5}$$

where κ_β and κ_ϕ are the scaling constants for $\overline{\beta}_{ai} = \kappa_\beta \beta_{ai}$, $\overline{\phi}_{ai} = \kappa_\phi \phi_{ai}$, $\overline{\beta}_{bi} = \kappa_\beta \beta_{bi}$, $\overline{\phi}_{bi} = \kappa_\phi \phi_{bi}$; $i = 1,2,...,m$. The adaptive parameters of neurons are defined as

$$\theta_i = [\alpha_{ai}, \beta_{ai}, \eta_{ai}, \phi_{ai}, \varphi_{ai}, \alpha_{bi}, \beta_{bi}, \eta_{bi}, \phi_{bi}, \varphi_{bi}] = [\theta_{i1}, ..., \theta_{i10}], \text{ for } i = 1,2,...,m, \tag{6}$$

where $\theta = [\theta_1, \theta_2, ..., \theta_m]^T$ is an adjustable parameter vector, and $I_p(t)$ is a feedforward term/input of the neurons. A complete scheme of the two-level feedforward control architecture is shown in Figure 1.

In this study, the proper adaptation laws with the projections are defined as follows.

$$\dot{\theta}_i = \begin{cases} \psi_i, & \text{if } (\|\theta_i\| < M_{\theta i}) \text{ or } (\|\theta_i\| = M_{\theta i} \text{ and } -\theta_i^T \psi_i \geq 0), \\ \text{Projection}(\psi_i), & \text{otherwise,} \end{cases} \tag{7}$$

where $\psi_i = \gamma_i E_i^T P_i \cdot B_{ci} \dfrac{\partial u_{Ci}}{\partial \theta_i}$, $\gamma_i > 0$; $\text{Projection}(\psi_i) = \psi_i - \dfrac{\theta_i}{\|\theta_i\|^2} \theta_i^T \psi_i$ for $i = 1,2,...,m$.

According to the parallel distributed rule and by substituting Eq. (2) into Eq. (1), we obtain

$$\begin{aligned} x_i^{(n_i)} &= f_i + c_i \cdot (u_{Ci} + u_{Si}) + c_i d_i = f_i + c_i \cdot (u_{Ci} + u_{Si}) + c_i u_i^* - c_i u_i^* + c_i d_i \\ &= f_i + c_i \cdot (u_{Ci} + u_{Si}) - f_i + y_{ri}^{(n_i)} + K_i^T E_i - c_i \cdot u_i^* + c_i d_i \\ &= y_{ri}^{(n_i)} + K_i^T E_i - c_i \cdot (u_i^* - u_{Ci} - u_{Si} - d_i). \end{aligned}$$

This implies that

$$e_i^{(n_i)} = -K_i^T E_i + c_i \cdot (u_i^* - u_{Ci} - u_{Si}) - c_i d_i. \tag{8}$$

Let

$$A_{ci} = \begin{bmatrix} 0_{(n_i-1)\times 1}, I_{(n_i-1)\times(n_i-1)} \\ -K_i^T \end{bmatrix} \text{ and } B_{ci} = [0_{2\times(n_i-1)}, c_i^T]^T \in \Re^{n_i \times 2} \tag{9}$$

be a companion form pair. From Eq. (8), we obtain

$$\dot{E}_i = A_{ci} E_i + B_{ci} (u_i^* - u_{Ci} - u_{Si} - d_i). \tag{10}$$

Here, we consider the Lyapunov function candidate

$$V_E = \sum_{i=1}^{m} V_{Ei}, \tag{11}$$

where $V_{Ei} = 2^{-1} E_i^T P_i \cdot E_i$ and $P_i > 0$ satisfy the Lyapunov equation

$$A_{ci}^T P_i + P_i \cdot A_{ci} = -Q_i, \tag{12}$$

and $Q_i > 0$ and $\lambda_{\min}(Q_i) > 1$, where $\lambda_{\min}(Q_i)$ denotes the minimum eigenvalue of Q_i.

We define

$$V_{Mi} = 2^{-1} \lambda_{\min}(P_i)(M_{Xi} - \|Y_{ri}\|_\infty)^2. \tag{13}$$

Here, $\|X_i\| \geq M_{Xi}$, then, from Eq. (11), $V_{Ei} \geq V_{Mi}$.

The time derivative of V_E along the trajectories of the closed-loop system of Eq. (10) satisfies

$$\dot{V}_E = \sum_{i=1}^{m}[2^{-1}E_i^T(A_{ci}^T P_i + P_i A_{ci})E_i + E_i^T P_i B_{ci}\cdot(u_i^* - u_{Ci} - u_{Si} - d_i)]$$

$$= -\sum_{i=1}^{m}[2^{-1}E_i^T Q_i E_i + E_i^T P_i B_{ci}(u_i^* - u_{Ci} - u_{Si} - d_i)]$$

$$\le -\sum_{i=1}^{m}[2^{-1}E_i^T Q_i E_i + |E_i^T P_i \cdot B_{ci}|(|u_i^*| + |u_{Ci} + d_{iU}|) - E_i^T P_i \cdot B_{ci}\cdot u_{Si}] \quad . \tag{14}$$

From Eq. (14), if there exists a supervisory control law with

$$u_{Si} = I_i^* \cdot \mathrm{sgn}(E_i^T P_i \cdot B_{ci})[|u_{Ci} + d_{iU}| + c_{iL}^+ \cdot (f_{iU} + |y_{ri}^{(n_i)}| + |K_i^T E_i|)], \tag{15}$$

where $c_{iL} \le c_i$ and f_{iU} is a boundary function for f_i such that $0 \le |f_i| \le f_{iU}$, then $\dot{V}_E < 0$ is guaranteed. Here, the indicator function I_i^* is defined by

$$I_i^* = \begin{cases} 1, & \text{for } V_{Ei} \ge V_{Mi}, \\ 0, & \text{otherwise.} \end{cases} \tag{16}$$

For the following deviation, the bounded generalized modeling error is defined as

$$e_{mi} = u_{Ci}(\theta_i^*) - u_i^* + d_i, \tag{17}$$

where θ_i^* is the optimal parameter vector. Then, Eq. (10) can be rewritten as

$$\dot{E}_i = A_{ci}E_i + B_{ci}u_{Ci}(\theta_i^*) - B_{ci}u_{Ci} - B_{ci}\cdot u_{Si} - B_{ci}e_{mi}. \tag{18}$$

From Taylor series expansions, we obtain

$$u_{Ci}(\theta_i^*) - u_{Ci}(\theta_i) = (\theta_i^* - \theta_i)^T \frac{\partial u_{Ci}(\theta_i)}{\partial \theta_i} + \varepsilon_i, \tag{19}$$

where ε_i is the approximation error of the higher order term.

Now, consider another Lyapunov function candidate containing the system error and the error between θ_i and θ_i^* given as

$$V = \sum_{i=1}^{m} V_i = \sum_{i=1}^{m}[2^{-1}E_i^T P_i E_i + (2\gamma_i)^{-1}(\theta_i - \theta_i^*)^T(\theta_i - \theta_i^*)] \quad . \tag{20}$$

Using Eqs. (18)–(20), we obtain

$$\dot{V} = \sum_{i=1}^{m}\{-2^{-1}E_i^T Q_i E_i + E_i^T P_i B_{ci}[u_{Ci}(\theta_i^*) - u_{Ci}(\theta_i) - u_{Si} - e_{mi}] + \gamma_i^{-1}(\theta_i^* - \theta_i)^T(\dot{\theta}_i^* - \dot{\theta}_i)\}$$

$$= \sum_{i=1}^{m} \{-2^{-1} E_i^T Q_i E_i - \gamma_i^{-1} (\theta_i^* - \theta_i)^T [\dot{\theta}_i - \gamma_i E_i^T P_i B_{ci} \frac{\partial u_{Ci}(\theta_i)}{\partial \theta_i}]$$

$$- E_i^T P_i B_{ci} (e_{mi} - \varepsilon_i) - E_i^T P_i B_{ci} u_{Si} + \gamma_i^{-1} (\theta_i^* - \theta_i)^T \dot{\theta}_i^* \}. \quad (21)$$

Furthermore, as $E_i(0)$ and $u_{Ci}(0)$ are bounded, and the projection method of the adaptation laws ensures $u_{Ci}(t)$, there exists a boundary function $\tilde{e}_i$ such that $\left| E_i^T P_i B_{ci} (e_{mi} - \varepsilon_i) \right| \le \tilde{e}_i$. Thus, we obtain

$$\dot{V} \le \sum_{i=1}^{m} \{ -2^{-1} E_i^T Q_i E_i + | E_i^T P_i B_{ci} (e_{mi} - \varepsilon_i) | \} \le \sum_{i=1}^{m} \{ -2^{-1} \lambda_{\min}(Q_i) \| E_i \|^2 + \tilde{e}_i \} . \quad (22)$$

This guarantees that $\dot{V} < 0$ if $\| E_i \| > \frac{\sqrt{\tilde{e}_i}}{\sqrt{2^{-1} \lambda_{\min}(Q_i)}}$. Equation (7) is obtained from the proper adaptation law. If Eq. (22) is satisfied, the system Eq. (1) is uniformly ultimately bounded (UUB) stable.

4. Experiments

In the following experiments, the forward Euler method with $t = k \cdot T_s$ and sampling time T_s =1 s was used, where k is a time sequence. The proposed control scheme was implemented on a prototype marker with two colors, i.e., blue and orange (*i*=1, 2), in its image identification system for guiding an omnidirectional robot. As shown in Figure 2 and discussed in the literature [15], the guiding robot system comprises a single marker, a group of LED modules serving as light disturbance, a photoresistor, and a Kinect sensor. Here, consider a first-order nonlinear MIMO system described as the following LED dimming system for imaging plant in this Section of Problem Formulation. Regulating the image process output $y = [RP\_blue,\ RP\_orange]^T$ of the closed-loop system to the desired output y_r is performed using the proposed control scheme. From this first-order nonlinear MIMO system, the function and gains of the supervisory control law Eq. (15), i.e., $f_{1U}(X_1)$ and $f_{2U}(X_2)$, are given as

$f_{1U} = 233.7885$ and $c_{1L} = [1,1]$; $f_{2U} = 303.8726$ and $c_{2L} = [1,1]$.

Moreover, $k_{10} = 3$ and $k_{20} = 3$ were selected. From Eq. (9), we have

$A_{c1} = -k_{10} = -3$ and $B_{c1} = c_1 = [1,1]$; $A_{c2} = -k_{20} = -3$ and $B_{c2} = c_2 = [1,1]$.

From Eq. (12), with $Q_1 = 6$, we have $P_1 = 1$, and, with $Q_2 = 6$, we have $P_2 = 1$. Here, $x(0) = [0,0]^T$, $M_{X1} = 1$, and $M_{X2} = 1$ were selected values. In designing the supervisory control law, $M_{\theta 1} = 349.7834$ and $M_{\theta 2} = 415.6142$ were selected values for Eq. (13), and $\gamma_1 = 0.1$ and $\gamma_2 = 0.01$ were given for the adaptation law Eq. (7). The control objective is to maintain the RP

vector around the desired vector $y_r = [0.59,\ 0.65]^T$ by RPI. Figure 3 shows a performance comparison of several related image processing strategies based on various LED lights.

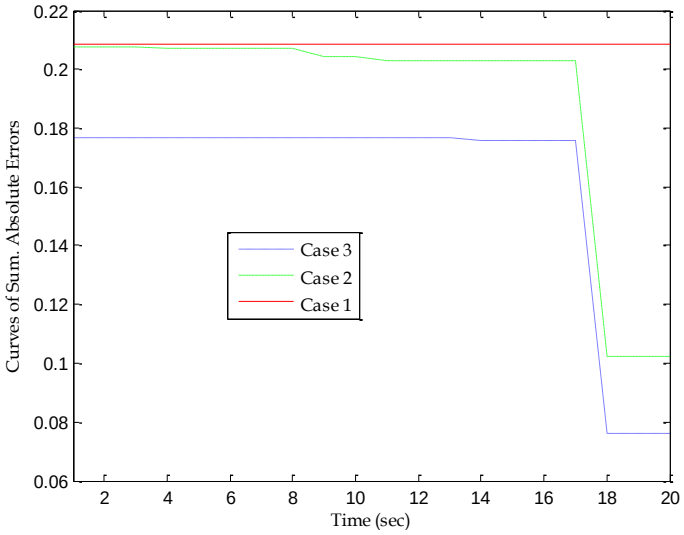

(a)

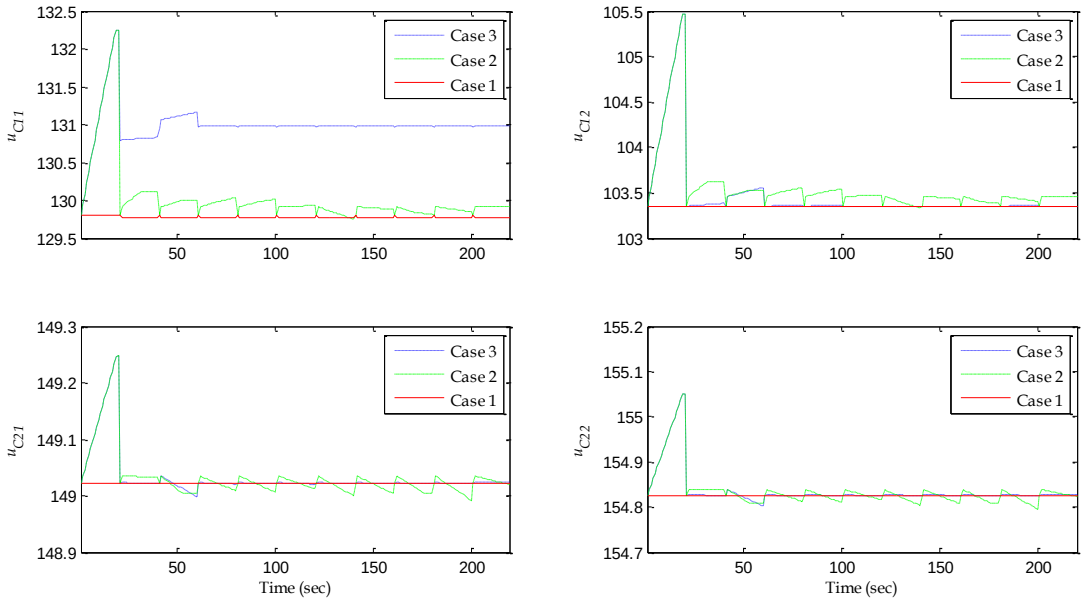

(b)

(c)

Figure 3. LED dimming equipment and Kinect image capturing system on three-wheeled omnidirectional robot [15] for marker identification by proposed adaptive image processing method (i.e., the DNC). (a) Experimental results (RPI) of the adaptive image processing system are based on varied LED lights (Cases 1－3). (b) Control input vector $u(t)$ of Cases 1－3. (c) Visible RP results of an adaptive marker for Case 3 under varying light intensity from multiple LED modules. The white line indicates the color identified region of interest, and its RP is optimized by the proposed adaptive control laws.

Case 1: Traditional static CIELab (Sab) color identification [23, 24] is an open-loop control structure. Here, "static" means that the parameters of the identifying colors cannot be adapted.

Case 2: Traditional dynamic CIELab (Dab) color identification [15] is a closed-loop control structure without feedforward input and piecewise adaptation.

Case 3: The proposed piecewise and dynamic CIELab color identification, which includes feedforward input ($\kappa_\beta = -0.02$; $\kappa_\phi = -0.3858$)

Figure 3 shows the trajectories of the control input and output response of the system when $\|\theta_1\|$ and $\|\theta_2\|$ are bounded by the UUB stabilization design and variations of the adaptation parameters are converged by the adaptation law. As shown in Figure 3a, the proposed scheme clearly demonstrates excellent identification performance compared to a traditional image processing method, and the feedforward term achieves further improvements. The analysis results shown in Figure 4 prove the validity of the proposed technique.

Journal of Engineering Technology

Volume 7, Special Issue (Internet of Things),Oct. 2018, PP. 145-158

RESEARCH ARTICLE -ENGINEERNG TECHNOLOGY ASEE

(a) (b)

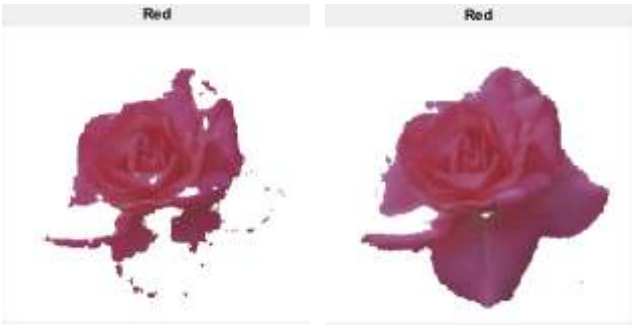

(c) (d)

Cases / Compared items	Case 1	Case 3
Identified pixels	20172 points in (c)	32279 points in (d)
$[a_1, b_1]$ for the red flower and $\begin{bmatrix} a_2, b_2 \\ a_3, b_3 \\ a_4, b_4 \end{bmatrix}$ for the other colors in (b).	$\begin{bmatrix} 188.1754, 140.6772 \\ 110.5964, 134.1827 \\ 133.4402, 119.5751 \\ 115.3214, 146.3571 \end{bmatrix}$	$\begin{bmatrix} 168.4417, 133.1422 \\ 110.5964, 134.1827 \\ 133.4402, 119.5751 \\ 115.3214, 146.3571 \end{bmatrix}$

(e)

Figure 4. (a) Training sample from benchmark database [24]. (b) Testing sample from benchmark database [24]. (c) Identifying the result of Case 1. (d) Identifying the result of Case 3. (e) Comparison of Cases 1 and 3.

5. Conclusion

In this study, we have proposed a robust adaptive control scheme for nonlinear image processing systems. An important contribution of the proposed scheme relates to the hardware implementations. This scheme is augmented with a supervising controller to enhance closed-loop system robustness,

and the adaptation law has neurons that include the feedforward effect. The proposed two-loop structure with feedforward intensity and feedback tracking error of the RP for the RPI works excellently. In addition, a design methodology based on Lyapunov analysis has been presented. The experimental results obtained from a practical image identification task show that the design procedure is conceptually unique and control performance is excellent compared to a traditional image processing method. The feedforward term also contributes to further performance improvement.

Acknowledgments

The authors thank the Ministry of Science and Technology, R.O.C. for its support under contracts MOST 107-2221-E-468-018 and 106-2221-E-468-023. Our gratitude also goes to Dr. Chun-San Wang and Michael Burton, editor, Asia University.

References

[1] Jyothula. H, KoteswaraRao. S, ValliKumari. V, "Image segmentation applying adaptive kernel possibilistic C-means with level set method - A cluster center initialization approach grounded on Cuckoo based search", Journal of Engineering Technology 2017; 6: 19-34.

[2] Teja. AR, Verma. V, Chakraborty. C, "A new formulation of reactive-power-based model reference adaptive system for sensorless induction motor drive", IEEE Transactions on Industrial Electronics 2015; 62: 6797-6808.

[3] Ayele. EA, Dhok. SB, "Interpolation-free sub-pixel motion estimation using optimal adaptive Kalman filtering technique: a survey", Journal of Engineering Technology 2018; 6(1): 194-208.

[4] Bensaada. M, "Design of optimal robust adaptive Neuro-Fuzzy inference controller using sliding mode approach for application to DC-DC converter", Journal of Engineering Technology 2018; 6(2): 443-455.

[5] Laurent Bitjoka, Martial Ndje, Alexandre T. Boum, Joseph Song-Manguelle, "Implementation of quadratic dynamic matrix control on arduino due ARM cortex-M3 microcontroller board", Journal of Engineering Technology 2017; 6(2): 682-695.

[6] Abderrahmen Ben Chaabene, Khira Ouelhazi, Anis Sellami, "Following control of MIMO uncertain systems application to a water desalination system supplied by photovoltaic source", Journal of Engineering Technology 2018; 6(1): 1-12.

[7] Mujtaba Jaffery, Sohaib Aslam, Moinuddin Ghauri, M. Shahzad Khuram, Sikandar Rafiq, Subhan Khan, "Real-time implementation of model predictive control on a 16-bit microcontroller for speed control of a DC motor", Journal of Engineering Technology 2018; 6(1): 415-434.

[8] Ali. M, CW. Ahn, Pant. M, "A robust image watermarking technique using SVD and differential evolution in DCT domain", International Journal for Light and Electron Optics 2015; 125: 428-434.

[9] C. Das, S. Panigrahi, VK. Sharma, KK. Mahapatra, "A novel blind robust image watermarking in DCT domain using inter-block coefficient correlation", International Journal of Electronics and Communications 2014; 68: 244-253.

[10] Zhang. Z, Li. F, Zhao. M, Zhang. L, Yan. S, "Robust neighborhood preserving projection by nuclear/L2,1-norm regularization for image feature extraction", IEEE Transactions on Image Processing 2017; 26:1607-1622.

[11] van den Berg. NS, Miwa. M, KleinJan. GH, Sato. T, Maeda. Y, van Akkooi. AC, Horenblas. S, Karakullukcu. B, van Leeuwen. FW, "(Near-infrared) Fluorescence-guided surgery under ambient light conditions: A next step to embedment of the technology in clinical routine", Annals of Surgical Oncology 2016; 23: 2586–2595.

[12] Fan. X, Shi. P, Ni. J, Li. M, "A thermal infrared and visible images fusion based approach for multitarget detection under complex environment", Mathematical Problems in Engineering 2014; 2015 (2015) 1-11.

[13] Pont-Tuset. J, Arbelaez. P, Barron. JT, Marques. F, Malik. J, "Multiscale combinatorial grouping for image segmentation and object proposal generation", IEEE Transactions on Pattern Analysis and Machine Intelligence 2017; 39: 128-140.

[14] Zheng. Y, Jeon. B, Xu. D, Wu. QM, Zhang. H, "Image segmentation by generalized hierarchical fuzzy C-means algorithm", Journal of Intelligent & Fuzzy Systems 2015; 28: 961-973.

[15] Tsai. ZR, "Robust Kinect-based guidance and positioning of a multidirectional robot by log-ab recognition", Expert Systems with Applications 2013; 8829: 1-14.

[16] Sun. H, Luş. H, Betti. R, "Identification of structural models using a modified artificial bee colony algorithm", International Journal of Computers and Structures 2013; 116: 59-74.

[17] Roberge. V, Tarbouchi. M, Labonté. G, "Comparison of parallel genetic algorithm and particle swarm optimization for real-time UAV path planning", IEEE Transactions on Industrial Informatics 2013; 9: 132-141.

[18] Martínez-Soto. R, Castillo. O, Castro. JR., "Genetic algorithm optimization for type-2 non-singleton fuzzy logic controllers", Studies in Computational Intelligence 2014; 547: 3-18.

[19] Qiu. M, Ming. Z, Li. J, Gai. K, Zong. Z, "Phase-change memory optimization for green cloud with genetic algorithm", IEEE Transactions on Computers 2015; 64: 3528-3540.

[20] del Mar Pérez. M, Ghinea. R, Rivas. MJ, Yebra. A, Ionescu. AM, Paravina. RD, Herrera. LJ, "Development of a customized whiteness index for dentistry based on CIELAB color space", Dental Materials 2016; 32: 461-467.

[21] McGrath. JR, Beck. M, Hill Jr. ME, "Replicating red: Analysis of ceramic slip color with CIELAB color data", Journal of Archaeological Science: Reports 2017; 14: 432-438.

[22] Chaudhary. A, Raheja. JL, "Bent fingers' angle calculation using supervised ANN to control electro-mechanical robotic hand", Computers & Electrical Engineering 2013; 39: 1-11.

[23] Xiao. K, Zardawi. F, Noort. RV, Yates. JM, Colour reproduction for advanced manufacture of soft tissue prostheses, Journal of Dentistry 2013; 2063: 1-9.

[24] Lin. PT, Lin. BR, "Fuzzy automatic contrast enhancement based on fuzzy C-means clustering in CIELAB color space. InMechatronic and Embedded Systems and Applications (MESA)." 12th IEEE/ASME International Conference on 2016 Aug 29;1-10.